591221

Reliability Analysis and Reliability-Based Design Optimization of Circular Composite Cylinders under Axial Compression

Report for Grant: NAG 1-2038

Period of Performance: May 2000 - May 2001

Principal Investigator:

Masoud Rais-Rohani, Ph.D., PE
Associate Professor
Department of Aerospace Engineering
Mississippi State University
Mississippi State, MS 39762

Phone: (662) 325-7294
Fax: (662) 325-7730
E-mail: masoud@ae.msstate.edu

Submitted to:

Mechanics and Durability Branch
Mail Stop 190
NASA Langley Research Center
Hampton, VA 23681

Abstract

This report describes the preliminary results of an investigation on component reliability analysis and reliability-based design optimization of thin-walled circular composite cylinders with average diameter and average length of 15 inches. Structural reliability is based on axial buckling strength of the cylinder. Both Monte Carlo simulation and First Order Reliability Method are considered for reliability analysis with the latter incorporated into the reliability-based structural optimization problem. To improve the efficiency of reliability sensitivity analysis and design optimization solution, the buckling strength of the cylinder is estimated using a second-order response surface model. The sensitivity of the reliability index with respect to the mean and standard deviation of each random variable is calculated and compared. The reliability index is found to be extremely sensitive to the applied load and elastic modulus of the material in the fiber direction. The cylinder diameter was found to have the third highest impact on the reliability index. Also the uncertainty in the applied load, captured by examining different values for its coefficient of variation, is found to have a large influence on cylinder reliability. The optimization problem for minimum weight is solved subject to a design constraint on element reliability index. The methodology, solution procedure and optimization results are included in this report.

Shell Buckling Analysis

The circular composite cylinders considered in this study fall under the general category of thin shell structures with the displacement field described by the first-order shear deformation theory formulated as

$$\begin{aligned} u(x,y,z) &= u_0(x,y) + z\phi_x(x,y) \\ v(x,y,z) &= v_0(x,y) + z\phi_y(x,y) \\ w(x,y,z) &= w_0(x,y) \end{aligned} \tag{1}$$

where u_0, v_0, w_0 represent the midplane displacements in x, y, z directions (see Fig. 1), respectively, and ϕ_x, ϕ_y describe rotations about the y and x axes, respectively.

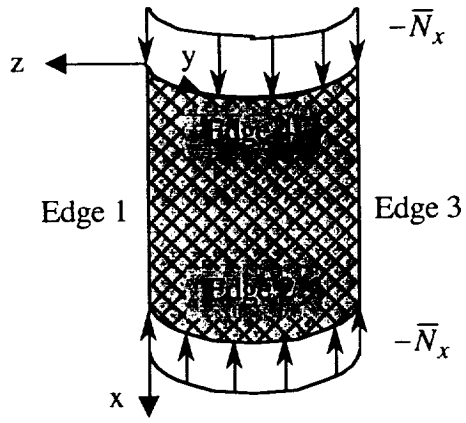

Fig. 1 Computational model used for cylinder buckling analysis

The strain-displacement relations are based on Sanders-Koiter shell theory with the in-plane strains ($\varepsilon_x^0, \varepsilon_y^0, \gamma_{xy}^0$, at $z = 0$), transverse shear strains ($\gamma_{xz}^0, \gamma_{yz}^0$, at $z = 0$), and curvatures ($\kappa_x, \kappa_y, \kappa_{xy}$) formulated as

$$
\begin{aligned}
\varepsilon_x^0 &= \frac{\partial u_0}{\partial x} \\
\varepsilon_y^0 &= \frac{\partial v_0}{\partial y} + \frac{w_0}{R} \\
\gamma_{xy}^0 &= \frac{\partial u_0}{\partial y} + \frac{\partial v_0}{\partial x} \\
\kappa_x &= \frac{\partial \phi_x}{\partial x} \\
\kappa_y &= \frac{\partial \phi_y}{\partial y} \\
\kappa_{xy} &= \frac{\partial \phi_x}{\partial y} + \frac{\partial \phi_y}{\partial x} + \frac{1}{2R}\left(-\frac{\partial u_0}{\partial y} + \frac{\partial v_0}{\partial x} \right) \\
\gamma_{xz}^0 &= \phi_x + \frac{\partial w_0}{\partial x} \\
\gamma_{yz}^0 &= \phi_y + \frac{\partial w_0}{\partial y} - \frac{v_0}{R}
\end{aligned}
\tag{2}
$$

where R is the shell radius of curvature in y direction (see Fig. 1). Hence, the elastic strain energy stored in the shell under axial compression can be expressed as

$$
U = \frac{1}{2}\int_A \{\varepsilon\}^T \begin{bmatrix} A_{ij} & B_{ij} & 0 \\ & D_{ij} & 0 \\ \text{sym} & & C_{pq} \end{bmatrix} \{\varepsilon\} dA \tag{3}
$$

where A_{ij}, B_{ij}, D_{ij} are the laminate extensional, coupling, and bending stiffness matrices, respectively, and C_{pq} is the transverse shear stiffness matrix with the strain vector defined as

$$
\{\varepsilon\}^T = \left\{ \varepsilon_x^0 \; \varepsilon_y^0 \; \gamma_{xy}^0 \; \kappa_x \; \kappa_y \; \kappa_{xy} \; \gamma_{xz}^0 \; \gamma_{yz}^0 \right\}^T \tag{4}
$$

The work done by the applied edge load shown in Fig. 1 can be expressed as

$$
W = \frac{1}{2}\int_A \overline{N}_x \left[\left(\frac{\partial v_0}{\partial x} \right)^2 + \left(\frac{\partial v_0}{\partial x} \right)^2 \right] dA \tag{5}
$$

where $\overline{N}_x$ is the stress resultant in the x direction.

To obtain the critical buckling load, the displacements u_0, v_0, w_0 and rotations ϕ_x, ϕ_y are approximated by different Ritz series with Legendre polynomials used as the interpolation functions such that the essential boundary conditions are satisfied. Then by applying the principle

of minimum total potential energy, the critical buckling load is found by setting Eqs. (3) and (5) equal to each other and solving the resulting eigenvalue problem for the critical load factor such that

$$N_{cr} = \lambda_{cr} N_x \tag{6}$$

A computer code (hereinafter referred to as the shell code) based on the described analysis procedure[1] is used to calculate the axial buckling loads for circular cylinders with clamped loaded edges. In this case, edge shortening is allowed along edge 4 with edge 2 kept fixed (see Fig. 1). Also the conditions of symmetry along edges 1 and 3 are enforced by setting the v displacement and ϕ_y rotation to zero. Table 1 below shows the list of boundary conditions.

Table 1. Description of boundary conditions for the shell model[a]

Parameter	Edge 1	Edge 2	Edge 3	Edge 4
u	0	1	0	0
v	1	1	1	1
w	0	1	0	1
ϕ_x	0	1	0	1
ϕ_y	1	1	1	1

[a] 0 = free, 1 = fixed

For validation purposes, we compared the results found using the shell code with those reported previously by Waters[2] as well as those we obtained using the STAGS structural analysis code. Table 2 below shows the geometric and material properties used for each specimen while Table 3 gives the laminate ply distribution and the corresponding cylinder buckling force.

Table 2. Geometric and material properties of each cylinder specimen

Specimen	L, in	D_1, in	t_{ply}, in	E_1, psi	E_2, psi	ν_{12}	G_{12}, psi
1	14	15.75	0.005	18.5111e6	1.64e6	0.3	0.8706e6
2	14	15.75	0.005	18.5780e6	1.64e6	0.3	0.8737e6
3	14	15.75	0.005	18.6705e6	1.64e6	0.3	0.8780e6
4	14	15.75	0.005	19.2588e6	1.64e6	0.3	0.9057e6
5	14	15.75	0.005	18.6154e6	1.64e6	0.3	0.8754e6

The results obtained from the shell code are in fairly good agreement with those found using STAGS. The difference ranges from the lowest (0.3%) for specimen 5 to the highest (17%) for specimen 1. The large difference observed in the case of specimen 1 may be attributed to using a Legendre polynomial that is not of sufficient accuracy for the selected ply pattern. We also observed some differences with the results found by Waters[2]. Of particular interest is the difference between specimens 4 and 5. We found cylinder 5 to be stronger of the two whereas the results obtained by Waters shows the opposite. Upon closer examination of both STAGS and shell code models, we did not find anything that would explain the reason for this discrepancy. However, it appears that for the case when the cylinder length and diameter are of nearly equal values, the laminate pattern reinforcing the hoop direction (specimen 5) provides a stiffer design than that reinforcing the axial direction (specimen 4). This response is attributed mainly to the Poisson's effect. Our results are consistent with the nonlinear static and nonlinear transient buckling analyses conducted by Hillburger and Starnes[3].

Table 3. Comparison of predicted and measured buckling loads

Specimen	Ply Distribution	Axial Buckling Force, lb				
		Linear FEA[a]	Non-Linear FEA[a]	Experiment[a]	STAGS[b]	Shell Code
1	$(\pm 45/0/90)_s$	44,466	39,670	30,164	42,355	49,553
2	$(\pm 45/\mp 45)_{2s}$	105,829	95,618	73,975	104,044	111,349
3	$(\pm 45/0/90)_{2s}$	158,258	-	147,759	180,443	185,420
4	$(\pm 45/0_4/\mp 45)_s$	141,332	128,610	125,542	154,655	158,319
5	$(\pm 45/90_4/\mp 45)_s$	139,411	97,047	91,667	167,175	167,717

[a]Values reported by Waters[2] using L = 16 in. with a 1 in. cap at each end.
[b]51 quadrilateral elements along the length and169 along the circumference.

Structural Reliability Analysis

The limit-state function for the critical axial buckling force is formulated as

$$g(X) = P_{cr} - P_a \tag{7}$$

where P_a is the resultant axial force (Load) acting on the cylinder, P_{cr} is the corresponding buckling force (Resistance), and $X = \{X_1, X_2, ..., X_n\}^T$ is the vector of continuous random variables affecting the buckling load. According to Eq. (7), $g < 0$ represents failure, $g > 0$ indicates safety, and $g = 0$ represents the limit-state surface separating the failure and safe regions.

The probability of failure is expressed mathematically as $P_f = P(g(X) \le 0)$, and found as

$$P_f = \int\int ... \int_{\Omega} f_X(x_1, x_2, ..., x_n) dx_1 dx_2 ... dx_n \tag{8}$$

where $f_X(x)$ is the joint probability density function of n random variables and Ω is the failure region defined by $g \le 0$.

Since the determination of the joint probability density function is not possible in this case, several alternative techniques may be used to estimate the probability of failure as defined by Eq. (8). Next we discuss two such techniques used in this investigation.

Monte Carlo Simulation

To estimate the failure probability using the Monte Carlo simulation (MCS) techniques, a large population of response samples must be obtained. Random sampling is done by using a random number generator to obtain the values for $X_1, X_2, ..., X_n$ based on the specified mean, variance, and distribution type of each random variable. Using each random set as input, the shell code is used to obtain the corresponding buckling load followed by the limit-state function in Eq. (7) at each simulation cycle. Hence, the failure probability and its corresponding coefficient of variation are found as

$$P_f = N_f / N \tag{9}$$

$$COV(P_f) = \sqrt{\frac{(1-P_f)P_f}{N}} \Big/ P_f \tag{10}$$

where N is the total number of simulation cycles, and N_f is the number of cycles resulting in "failure" ($g \le 0$). The estimates obtained for P_f and $COV(P_f)$ become exact as N approaches infinity.

In this study, we treated the applied load, geometric dimensions of the cylinder, and engineering properties of the material as random with statistical properties as defined in Table 4. The material properties correspond to carbon/epoxy (AS4 12k/3502) unidirectional tape with nominal engineering properties obtained from MIL-HDBK-17-2E. Due to unavailability of data, the coefficients of variation in the applied load and geometric variables are assumed. All random variables are also assumed to be statically independent. The shell laminate contains 16 layers each defined by separate thickness and ply angle variables. Therefore, Table 4 describes a total of 39 random variables.

Table 4. Statistical properties of random variables affecting cylinder reliability

Random Variable (No)	Distribution Type	Mean	COV (%)
E_1 (1)	Normal	18.0e6 psi	3.19
E_2 (2)	Normal	1.35e6 psi	4.26
ν_{12} (3)	Normal	0.226	5
G_{12} (4)	Normal	0.543e6 psi	5.16
t_{ply} (5-20)	Normal	0.005 in.	1
θ_{ply} (21-36)	Normal	$[\pm 45/90_4/\mp 45/\pm 45/90_4/\mp 45]$	1[a]
D (37)	Normal	15 in.	1
L (38)	Normal	14 in.	1
P_a (39)	Normal	14.369e4 lb	5

[a]Standard Deviation

Of a total of 5,314 simulation cycles conducted, buckling failure (i.e., $g \le 0$) was observed in 988 samples. This gives a probability of failure $P_f = 0.186$ for this specimen based on the assumed mean and variance for the resultant compressive axial load. The plots of P_f and COV are shown in Fig. 2 with the coefficient of variation conversing to $COV(P_f) = 0.0287$.

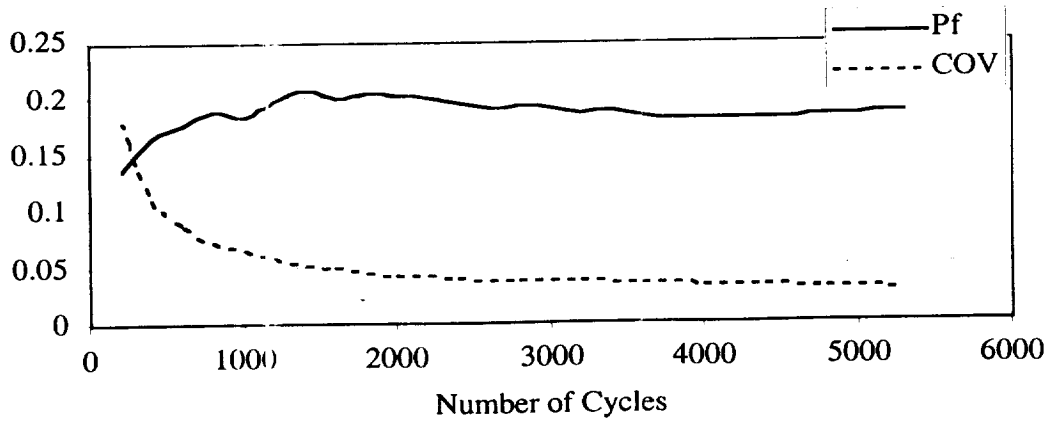

Fig. 2 MCS convergence history

The histogram for the buckling load P_{cr} in Fig. 3 shows a normal probability distribution with a mean of 151,203 lb and a coefficient of variation of 2.8% (standard deviation of 4,245 lb).

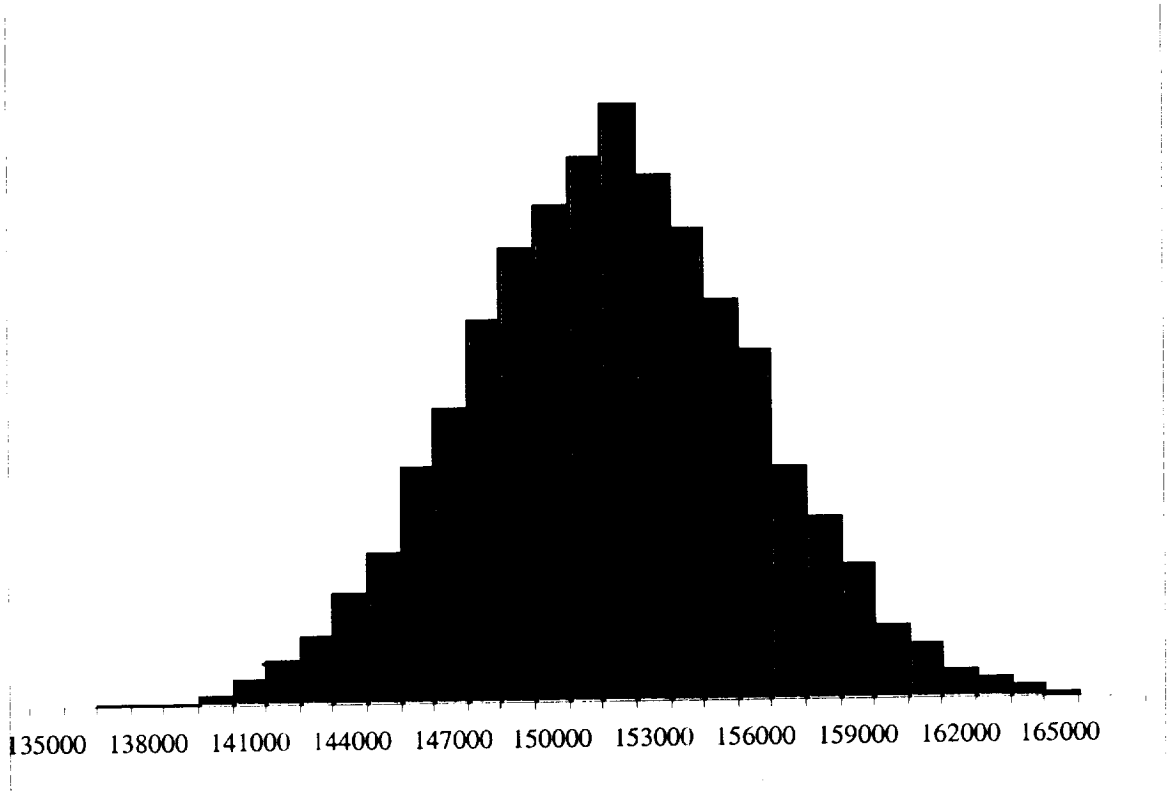

Fig. 3 Histogram for axial buckling force, P_{cr}(lb)

In examining the effect of the coefficient of variation of the external force (i.e., COV(P_a)) on cylinder failure probability, we found that in changing the COV from 1% to 10%, failure probability increases from $P_f = 0.05$ to $P_f = 0.308$, an increase of 516%.

Although Monte Carlo simulation provides a convenient technique for the estimation of failure probability, it may be very inefficient when considering the computational time associated with each buckling analysis. A more efficient alternative to MCS involves the use of analytical techniques as discussed in next.

Reliability Index

If the limit state function is a linear function of all random variables, then we can use the first-order reliability method (FORM) to calculate the so called reliability index β as the inverse of the coefficient of variation of the limit state function or simply

$$\beta = \frac{\mu_{P_{cr}} - \mu_P}{\sqrt{\sigma_{P_{cr}}^2 + \sigma_P^2}} \tag{11}$$

where $\mu_{P_{cr}}$, μ_P are the mean values of the critical axial buckling force and resultant axial force, respectively, and $\sigma_{P_{cr}}$, σ_P are the corresponding standard deviations. Since $P_{cr} = P_{cr}(\boldsymbol{X})$, and all the random variables are assumed to be uncorrelated, we can obtain the variance of the buckling force using the partial derivative rule

$$\sigma_{P_{cr}}^2 = \sum_{i=1}^{n}\left(\frac{\partial P_{cr}}{\partial X_i}\right)^2 \sigma_{X_i}^2 \tag{12}$$

If an analytical expression relating P_{cr} to the pertinent random variables is available, then the partial derivatives in Eq. (12) can be obtained analytically, otherwise they may be found numerically using a finite difference scheme.

If all random variables are normally distributed, then the probability of failure can be found as

$$P_f = \Phi(-\beta) \tag{13}$$

where Φ is the cumulative distribution function of the standard normal variate. For example, $\beta = 4.26$ would correspond to $P_f \approx 10^{-5}$.

If, on the other hand, the limit state function is a nonlinear function of random variables, then the method proposed by Hasofer and Lind[4] may be used to solve for β. In this method, the original limit state, $g(\boldsymbol{X}) = 0$, is transformed into the reduced limit state, $g(\boldsymbol{X}') = 0$, with each reduced random variable found using the transformation

$$X'_i = \frac{X_i - \mu_{X_i}}{\sigma_{X_i}}, \qquad i = 1,2\ldots,n \tag{14}$$

The point on the reduced limit-state surface $g(\boldsymbol{X}') = 0$ having the maximum joint probability of failure is called the design point (also known as the most probable failure point, MPP) with coordinates identified by vector $\boldsymbol{x}'^*$. The distance from the origin of the reduced coordinate system to the design point is the shortest distance to the failure surface, and is identified as β or the Hasofer-Lind reliability index. Each coordinate of the design point is related to the reliability index as

$$x'^*_i = -\alpha_i^* \beta, \qquad i = 1,2,\ldots,n \tag{15}$$

where α_i^* represents the direction cosine corresponding to X'_i, and is found as

$$\alpha_i^* = \left(\frac{\partial g}{\partial X'_i}\right)_* \Bigg/ \sqrt{\sum_{j=1}^{n}\left(\frac{\partial g}{\partial X'_j}\right)_*^2}, \quad i,j = 1,2,\ldots,n \tag{16}$$

The asterisk symbol indicates that the derivatives of the reduced limit-state function are evaluated at the design point. Since the limit-state function is nonlinear, the solution for β becomes iterative as described in the appendix.

Reliability Sensitivity Analysis

A useful by product of analytical reliability technique is the evaluation of probabilistic sensitivity derivatives of β with respect to the mean μ_{X_i} and standard deviation σ_{X_i} of each random variable as

$$\frac{\partial \beta}{\partial \mu_{X_i}} = -\frac{x'^*_i}{\beta \sigma_{X_i}} = \frac{\alpha^*_i}{\sigma_{X_i}}, \quad i = 1,2,...,n \tag{17}$$

$$\frac{\partial \beta}{\partial \sigma_{X_i}} = -\frac{x'^{*2}_i}{\beta \sigma_{X_i}} = \frac{\alpha^*_i x'^*_i}{\sigma_{X_i}}, \quad i = 1,2,...,n \tag{18}$$

Since the random variables (see Table 4) are of vastly different scales, the sensitivity derivatives are normalized as

$$\delta_i = \frac{\partial \beta}{\partial \mu_{X_i}} \left(\frac{\mu_{X_i}}{\beta} \right) \tag{19}$$

$$\eta_i = \frac{\partial \beta}{\partial \sigma_{X_i}} \left(\frac{\sigma_{X_i}}{\beta} \right) \tag{20}$$

To calculate β and its sensitivity derivatives, we must be able to evaluate the derivatives of the limit-state function with respect to individual random variables. These calculations, whether the limit-state function is linear or nonlinear, become very time consuming if there are many random variables and if $g(X)$ is an implicit function of these random variables.

To alleviate this burden and facilitate the subsequent reliability-based design optimization, we developed an analytical model of the limit-state function using the response surface methodology as discussed next.

Response Surface Methodology

Response surface methodology (RSM) is mainly a statistical procedure used to develop a smooth mathematical function that represents an accurate functional relationship between the response variable and the independent parameters that influence it.

A quadratic response surface model for n independent variables can be expressed as

$$f(\boldsymbol{X},\boldsymbol{a}) = a_0 + \sum_{i=1}^{n} a_i X_i + \sum_{i=1}^{n} \sum_{j=1}^{i} a_{ij} X_i X_j \tag{21}$$

where a_0, a_i, a_{ij} are the unknown regression parameters for a total of $(n+1)(n+2)/2$ including the interaction terms $X_i X_j$, $i \neq j$. The accurate estimation of these regression parameters usually requires a large number of response samples, which could significantly increase the computational cost of the analysis.

For estimation of cylinder reliability, we replaced the exact limit-state function in Eq. (7) by a close approximation in the form

$$\tilde{g}(X) = \tilde{P}_{cr} - P_a \tag{22}$$

where $\tilde{P}_{cr}$ is the estimated (fitted) axial buckling force found using the algebraic response surface model defined by Eq. (21).

For the cylinder specimen described in Table 4, we estimated the coefficients a_0, a_i, a_{ij} by performing a least-squares fit of the regression model in Eq. (21) to the response values obtained from the Monte Carlo simulation.

To validate the model, we examined various statistics such as the coefficient of determination R^2 and the root mean square error (RMSE) found as

$$RMSE = \sqrt{\frac{\sum_{i=1}^{N}\left(P_{cr_i} - \tilde{P}_{cr_i}\right)^2}{N - M}} \tag{23}$$

where N is the number of response observations and M is the number of unknown coefficients in the response surface model.

Since the approximate limit-state function in Eq. (22) is an explicit function of all 39 random variables, we would be able to calculate β and its probabilistic sensitivities through analytical differentiation of the response surface model. The mean buckling force estimated by the second order response surface equation is found to be 151,203 lb with model RMSE = 150.85 lb and R^2 = 0.9989.

Table 5 below shows the values of the sensitivity derivatives of β with respect to the mean and standard deviation of each random variable. The values in columns 3 and 5 are the normalized or logarithmic sensitivity derivatives that are normalized once more with respect to the largest sensitivity value in each group.

As highlighted in Table 5, of all random variables, the applied load, Young's modulus in the fiber direction, and cylinder diameter are found to have the greatest influence on cylinder reliability with axial buckling as the only failure mode. Although total shell thickness does have a large impact on cylinder buckling, the influence of each individual ply thickness is found to be less significant. It is also important to point out that the probabilistic sensitivity derivatives of β are greatly influenced by the variance in each random variable both implicitly and explicitly as indicated by Eqs. (17) and (18).

Table 5. Probabilistic sensitivity derivatives of reliability index β for the specimen in Table 4

Random Variable	$(\partial\beta / \partial\mu_{X_i})$	$(\delta_i)_{\text{norm}}$	$(\partial\beta / \partial\sigma_{X_i})$	$(\eta_i)_{\text{norm}}$
E_1	8.14E-07	**8.44E-01**	-3.53E-07	**-2.90E-01**
E_2	1.68E-06	1.30E-01	-1.50E-07	-1.24E-02
ν_{12}	6.92E-01	9.01E-03	-5.03E-03	-8.11E-05
G_{12}	2.52E-06	7.87E-02	-1.65E-07	-6.60E-03
t_1	4.13E+02	1.19E-01	-7.93E+00	-5.66E-04
t_2	4.40E+02	1.27E-01	-9.01E+00	-6.43E-04
t_3	4.02E+02	1.16E-01	-7.49E+00	-5.35E-04
t_4	4.10E+02	1.18E-01	-7.81E+00	-5.58E-04
t_5	4.05E+02	1.17E-01	-7.62E+00	-5.44E-04
t_6	3.93E+02	1.13E-01	-7.17E+00	-5.12E-04
t_7	4.42E+02	1.27E-01	-9.06E+00	-6.47E-04
t_8	5.80E+02	1.67E-01	-1.56E+01	-1.11E-03
t_9	5.63E+02	1.62E-01	-1.47E+01	-1.05E-03
t_{10}	4.50E+02	1.30E-01	-9.40E+00	-6.71E-04
t_{11}	3.46E+02	9.95E-02	-5.55E+00	-3.96E-04
t_{12}	3.38E+02	9.73E-02	-5.31E+00	-3.79E-04
t_{13}	3.42E+02	9.85E-02	-5.44E+00	-3.88E-04
t_{14}	3.52E+02	1.03E-01	-5.75E+00	-4.10E-04
t_{15}	5.28E+02	1.52E-01	-1.29E+01	-9.23E-04
t_{16}	5.12E+02	1.47E-01	-1.22E+01	-8.70E-04
θ_1	-3.33E-02	-8.63E-02	-4.63E-04	-2.98E-04
θ_2	-2.79E-02	7.22E-02	-3.25E-04	-2.09E-04
θ_3	2.53E-02	1.31E-01	-5.36E-04	-6.88E-04
θ_4	1.86E-02	9.61E-02	-2.88E-04	-3.70E-04
θ_5	1.27E-02	6.61E-02	-1.36E-04	-1.75E-04
θ_6	7.92E-03	4.10E-02	-5.24E-05	-6.74E-05
θ_7	1.08E-02	-2.79E-02	-4.84E-05	-3.11E-05
θ_8	-4.49E-02	-1.16E-01	-8.43E-04	-5.42E-04
θ_9	-4.42E-02	-1.15E-01	-8.19E-04	-5.25E-04
θ_{10}	2.44E-02	-6.32E-02	-2.48E-04	-1.60E-04
θ_{11}	-2.43E-03	-1.26E-02	-4.95E-06	-6.36E-06
θ_{12}	-2.50E-03	-1.29E-02	-5.21E-06	-6.69E-06
θ_{13}	-1.43E-03	-7.42E-03	-1.71E-06	-2.20E-06
θ_{14}	-6.82E-05	-3.54E-04	-4.05E-09	-5.20E-09
θ_{15}	3.95E-02	-1.02E-01	-6.52E-04	-4.19E-04
θ_{16}	-4.35E-02	-1.13E-01	-7.90E-04	-5.07E-04
D	2.85E-01	**2.46E-01**	-1.13E-02	**-2.43E-03**
L	-1.85E-01	-1.49E-01	-4.46E-03	-8.92E-04
P_a	-1.21E-04	**-1.00E+00**	-9.75E-05	**-1.00E+00**

Figure 4 gives the plots of normalized sensitivity derivatives of β with respect to mean and standard deviation of each random variable.

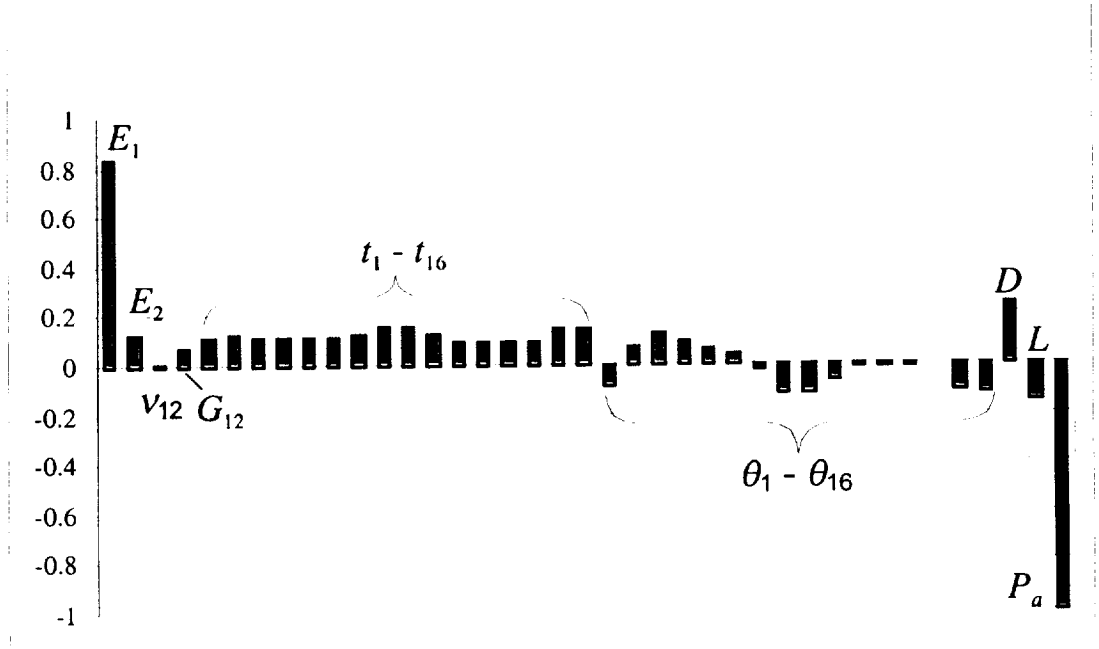

(a)

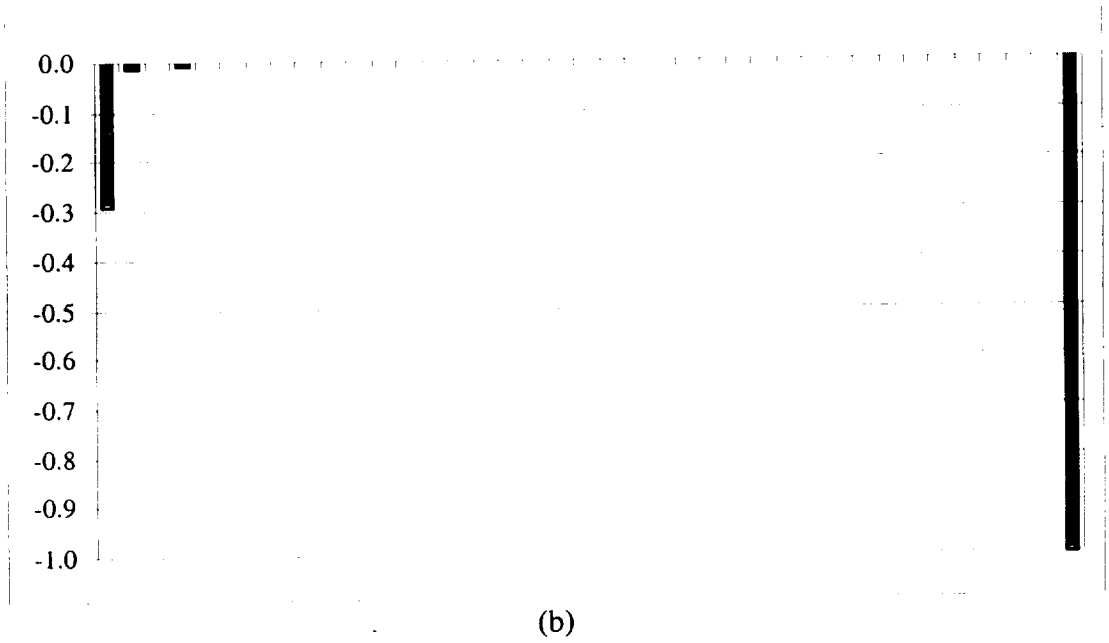

(b)

Fig. 4 Normalized probabilistic sensitivities of β with respect to (a) mean value and (b) standard deviation of each random variable for the specimen defined in Table 4

Effects of Distribution and Coefficient of Variation of Applied Load on β

Since the results of reliability analysis indicated a large sensitivity to the applied load, we also examined the effects of the distribution type and coefficient of variation of P_a on β and probability of failure. Two different distribution types (Normal and Lognormal) and three different values for coefficient of variation of P_a were considered. In both cases, the applied load was assumed to have a mean of 143,690 lb. The critical buckling load was determined from the response surface model and was not affected by changes in COV of the applied load.

The results shown in Table 6 below indicate that the coefficient of variation has a significant influence on both β and probability of failure whereas the effect of the distribution type is relatively insignificant. It must be noted that in both cases the remaining 38 random variables were assumed to have normal distributions as specified in Table 4.

Table 6. The effects of distribution and coefficient of variation of P_a on cylinder reliability

		Reliability Index Method		Monte Carlo Simulation
P_a Distribution	COV (%)	β	P_f	P_f
Normal	1	1.7315	0.042	0.050
	5	0.9099	0.181	0.186
	10	0.5038	0.309	0.308
Lognormal	1	1.7326	0.042	0.050
	5	0.9188	0.179	0.184
	10	0.5421	0.295	0.295

Reliability-Based Structural Optimization

The optimization problem is formulated as an element reliability index based structural optimization problem with a single design constraint imposed on buckling reliability index. Mathematical y, the optimization problem may be formulated as

$$\begin{aligned} &\text{minimize } W(\boldsymbol{X}) \\ &\text{subject to: } \beta_b \geq \beta_{\min} \\ &\qquad Y_i^l \leq Y_i \leq Y_i^u, \qquad i = 1,2,\ldots,NDV \end{aligned} \tag{24}$$

where W is the cylinder weight and β_b is the reliability index associated with axial buckling. The design variables represent the mean values of only a subset of random variables such that $Y_i = \mu_{X_i}$ with the corresponding standard deviations held constant during the optimization process. Each design variable is limited by lower and upper bound side constraints as indicated in Eq. (24).

We chose a laminate concept similar to that in Table 4, but with midplane symmetry (i.e., $[\pm 45 / 90_4 / \mp 45]_s$), which reduces the total number of random variables from 39 to 23. Of the total of 23, only the 8 corresponding to ply thicknesses are treated as design variables. More specifically, their mean values are allowed to change while their standard deviations are held fixed. The mean thickness for each ply is limited by lower and upper bounds of 0.0026 in. and 0.007 in., respectively.

The other geometric parameters and material properties (in Table 4) are treated as random but with their means and coefficients of variation kept fixed during the optimization process.

The optimization problem in Eq. (24) is solved using the method of sequential quadratic programming in DOT[5] optimization software based on a global response surface modeling of the buckling response as explained next.

Global Response Surface Technique

In this case, a quadratic response surface model similar to that in Eq. (21) is developed for use over the entire design space. The population responses are generated using a direct Monte Carlo simulation with each random variable having a uniform distribution defined by the limits

$$X_j^u,\ X_j^l = (1 \pm \varsigma_{X_j})\mu_{X_j}, \qquad j = 1,2,...,n \tag{25}$$

where ς_{X_j} represents the bound increment for random variable X_j as defined in Table 7 below.

By assuming each random variable is uniformly distributed, we are attempting to obtain samples from various points in the design space. This modeling of random variables, however, would not prevent the use of the resulting response surface model for design optimization where individual random variables are assumed to have a normal distribution.

Table 7. Mean values and bound increments of random variables in Monte Carlo simulation

Random Variable (X_j)	μ_{X_j}	ς_{X_j} (%)
Elastic Modulus, E_1	18.0e6 psi	4
Elastic Modulus, E_2	1.35e6 psi	5
Poisson Ratio, ν_{12}	0.226	6
Shear Modulus, G_{12}	0.543e6 psi	6
Ply Thickness, t_{ply}	0.005 in.	50
Ply Angle, θ_{ply}	45°, -45°, or 90°	26
Cylinder Diameter, D	15 in.	50
Cylinder Length, L	15 in.	50

The large increment on ply thickness allows for sampling over the entire feasible design space consistent with the corresponding lower and upper bounds specified in the optimization problem. We also chose large increments for cylinder diameter and length so the same response surface model can be used for optimization of cylinders with length and diameter of 10 to 20 in. Lastly, the support condition at the loaded edges is treated as deterministic with the external load assumed to be uniformly distributed over the top and bottom edges of the cylinder.

We generated the necessary response data by conducting a total of 3,588 Monte Carlo simulation cycles. The buckling response for each cycle is found using the shell code[1] with each interpolation function modeled by a 12th degree Legendre polynomial. The buckling load found directly from this computer program is dubbed herein as "exact".

The response surface model fitted through the sample data is found to have $R^2 = 0.9774$, COV = 3.04%, and RMSE = 4,383.26 lb. To assure the accuracy of the response surface model, we considered 20 random samples and compared the fitted buckling load to the exact value for each

sample. The results, shown in Table 8 below, indicate a maximum error of 4.22%, which is considered acceptable.

Table 8. Comparison of exact and fitted buckling loads

Random Sample	Exact P_{cr}, lb	Fitted $\tilde{P}_{cr}$, lb	% Error
1	148551	154305	3.87
2	164791	164622	0.10
3	157294	156206	0.69
4	155613	157132	0.98
5	146943	148753	1.23
6	154598	153307	0.84
7	147618	150250	1.78
8	157701	153539	2.64
9	149712	151621	1.28
10	152033	150656	0.91
11	138397	136995	1.01
12	149330	148239	0.73
13	149616	152113	1.67
14	124890	130162	4.22
15	138740	139190	0.32
16	157662	159231	1.00
17	160469	160284	0.12
18	148128	145619	1.69
19	154835	156182	0.87
20	143155	146534	2.36

Having developed the necessary response surface model, the optimization problem is solved with the mean and coefficient of variation of each random variable as specified in Table 9. The solution to the optimization problem is given in Table 10 for three combinations of length and diameter and two different values for coefficient of variation of the applied load. The minimum reliability index is chosen as 4.26. The total shell thickness, h is shown in Table 10 in lieu of each mean ply thickness value.

In all cases, the increase in COV (P_a) causes an increase in the optimal laminate thickness and cylinder weight. The combination of small diameter and long length increases the buckling strength of the cylinder. The large value for β_{min} resulted in many of the thickness design variables to be pushed closer to the upper bound of 0.007 in.

Table 9. Statistical properties of random variables used in cylinder design optimization

Random Variable	Dist. Type	Mean	COV (%)
P_a	Normal	143,690 lb	10
E_1	Normal	18.0e6 psi	3.19
E_2	Normal	1.35e6 psi	4.26
ν_{12}	Normal	0.226	5
G_{12}	Normal	0.543e6 psi	5.16
t_{ply}	Normal	μ_{Y_i}	5
θ_{ply}	Normal	$[\pm 45/90_4/\mp 45]_s$	5[a]
D	Normal	10, 15, 20 in.	10
L	Normal	10, 15, 20 in.	10

[a]Standard Deviation

Table 10. Optimization results for $\beta_{min} = 4.26$

Parameter	COV = 5%	COV = 10%
	$\mu_D = 20$ in., $\mu_L = 10$ in.	
$\tilde{P}_{cr}$, lb	200,278	223,995
W, lb	3.323	3.542
h, in	0.0924	0.0986
	$\mu_D = \mu_L = 15$ in.	
$\tilde{P}_{cr}$, lb	194,019	220,142
W, lb	3.692	3.956
h, in	0.0912	0.0976
	$\mu_D = 10$ in., $\mu_L = 20$ in.	
$\tilde{P}_{cr}$, lb	210,187	230,097
W, lb	3.601	3.790
h, in	0.0996	0.1046

Computational Requirements

Although the use of response surface model results in a considerable computational efficiency, it still requires further improvement. In this investigation, the major cost of the reliability-based design optimization was associated with the Monte Carlo simulation to generate the necessary pool of response samples for developing a reasonably accurate response surface model of the buckling load. Once that part of the problem was completed, the actual optimization analysis took no more than one or two minutes.

The 3,588 simulation cycles took approximately 448.5 CPU hours on a Sun server. Therefore, it is clear that other techniques for further improvement in computational efficiency must be investigated.

References

1. Jaunky, N., Knight, N., "An Assessment of Shell Theories for Buckling of Cylindrical Panels," *International Journal of Solid Structures,* Vol. 36, 1999, pp. 3799-3820.

2. Waters, A.W., Jr., "Effects of Initial Geometric Imperfections on the Behavior of Graphite-Epoxy Cylinders Loaded in Compression," MS Thesis, Department of Engineering Mechanics, Old Dominion University, 1996.

3. Hillburger, M. W. and Starnes, Jr., J. H., "High-Fidelity Nonlinear Analysis of Compression-Loaded Composite Shells," Proceedings of the 42nd AIAA/ASME/ASCE/AHS/ASC Structures, Structural Dynamics, and Materials Conference, Seattle, WA, Apr. 16-19, 2001, AIAA Paper No. 2001-1394.

4. Hasofer, A.M. and Lind, N., "An Exact and Invariant First-Order Reliability Format," *Journal of Engineering Mechanics*, Vol. 100, No. EM1, 1974, pp. 111-121.

5. DOT optimization software (Version 5.0), Vanderplaats Research and Development, Inc. 1995.

6. Ayyub, B. M., and McCuen, R. H., Probability, Statistics, and Reliability for Engineers, CRC Press, 1997, pp. 406-408.

Appendix

For the composite cylinder, the nonlinear limit state function is expressed as $g(x_1'^*, x_2'^*, \ldots x_n'^*)$ where $(x_1'^*, x_2'^*, \ldots x_n'^*)$ represent the reduced coordinates of the design point (or MPP), which are unknown initially, and are calculated according to the iterative process outlined in Fig. A-1.

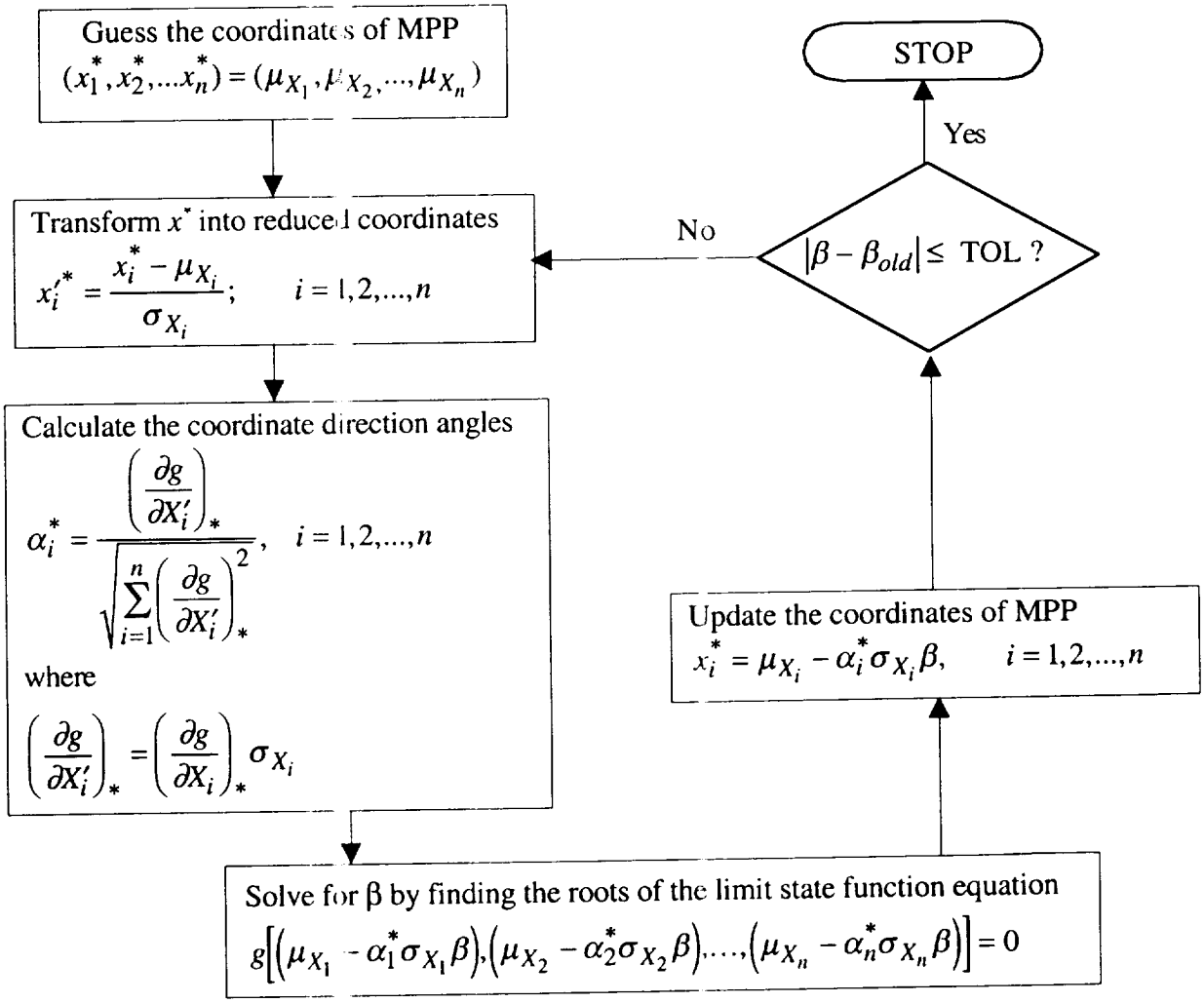

Fig. A-1 Procedure for calculating the Hasofer-Lind reliability index

For a more thorough description of the procedure, the reader is referred to Refs. 4 and 6.